This article has been accepted for publication in a future issue of this journal, but has not been fully edited. Content may change prior to final publication. Citation information: DOI 10.1109/JSTARS.2020.2992530, IEEE Journal of Selected Topics in Applied Earth Observations and Remote Sensing

Modeling and Compensation of the Penetration Bias in InSAR DEMs of Ice Sheets at Different Frequencies

Georg Fischer, *Member, IEEE*, Konstantinos P. Papathanassiou, *Fellow, IEEE*, and Irena Hajnsek, *Fellow, IEEE*

Abstract—Synthetic Aperture Radar Interferometry (InSAR) is able to provide important information for the characterization of the surface topography of glaciers and ice sheets. However, due to the inherent penetration of microwaves into dry snow, firn, and ice, InSAR elevation models are affected by a penetration bias. The fact that this bias depends on the snow and ice conditions as well as on the interferometric acquisition parameters complicates its assessment and makes it also relevant for measuring topographic changes. Recent studies indicated the potential for model based compensation of this penetration bias. This paper follows this approach and investigates the performance of two subsurface volume models for this task. Single-channel and polarimetric approaches are discussed for random and oriented volume scenarios. The model performance is assessed on two test sites in the percolation zone of the Greenland ice sheet using fully polarimetric airborne X-, C-, L-, and P-band InSAR data. The results indicate that simple models are able to partially compensate the penetration bias and provide more accurate topographic information than the interferometric phase center measurements alone.

***Index Terms*—Polarimetric Synthetic Aperture Radar Interferometry, microwave penetration, digital elevation model, glaciers, topography**

I. INTRODUCTION

DIGITAL elevation models (DEMs) of ice sheets derived during dry and frozen conditions from interferometric synthetic aperture radar (InSAR) measurements are affected by a bias, due to the penetration of microwave signals into snow, firn, and ice. The penetration bias is the difference between the surface elevation and the elevation of the interferometric phase center, which is located in the subsurface. In other words, the penetration bias in an InSAR DEM corresponds to the depth of the interferometric phase center. This depth depends on the snow and ice conditions, like the presence of refrozen ice inclusions within the firn, as well as on the acquisition parameters, i.e., polarization, frequency, incidence angle and interferometric baseline [1], [2]. Values of -1 m to -10 m at X-band (in the transition from the percolation to the dry snow zone in Greenland) [3], down to -13 m at C-band (with decreasing trend with increasing elevation in the percolation zone) [4], and -14 m at L-band (Greenland Summit) [5], with rare cases down to -120 m (cold marginal ice) [5], have been reported. These values indicate that the penetration bias can dominate the uncertainties in mass balance estimations of glaciers and ice sheets [6] derived from InSAR DEMs [3]. Even more so, the seasonal and long term changes of geophysical subsurface properties as well as variations in interferometric acquisition geometry can make a direct interpretation of elevation changes in InSAR DEMs difficult. The penetration bias, and its temporal change, can be of the same order than the occurring surface elevation change. Therefore, the estimation and compensation of the penetration bias becomes essential.

Different approaches have been followed to address the bias by using indicators of constant penetration bias [7], selected acquisitions during melting periods in order to minimize penetration [8], or empirically derived bias estimates [6], [9]. However, the spatial and temporal differences in penetration, as well as the dependence of the bias on the interferometric baseline hamper these approaches. An alternative option to account for the bias is the use of scattering models. First studies indicated the potential of a model based estimation of the phase center depth directly from (polarimetric) InSAR data [1]. This paper follows this approach and investigates the ability of simple subsurface volume models to estimate and compensate the penetration bias.

A successful bias compensation has to consider four aspects. First, its absolute value, in case InSAR surface elevations are compared to DEMs derived from optical data or radar altimetry. Second, the temporal changes of the bias that are relevant for comparing InSAR DEMs acquired at different dates. Third, differences in penetration in InSAR DEMs

Manuscript submitted for review Month, Day, Year. This work is supported by the Initiative and Networking Fund of the Helmholtz Association, in the frame of the 'Helmholtz Alliance Remote Sensing and Earth System Dynamics'

G. Fischer, K. P. Papathanassiou, and I. Hajnsek are with the Microwaves and Radar Institute (HR), German Aerospace Center (DLR), 82234 Wessling, Germany. (e-mail: georg.fischer@dlr.de; kostas.papathanassiou@dlr.de; irena.hajnsek@dlr.de)

G. Fischer and I. Hajnsek are also with the ETH Zurich, 8092 Zurich, Switzerland.

This article has been accepted for publication in a future issue of this journal, but has not been fully edited. Content may change prior to final publication. Citation information: DOI 10.1109/JSTARS.2020.2992530, IEEE Journal of Selected Topics in Applied Earth Observations and Remote Sensing

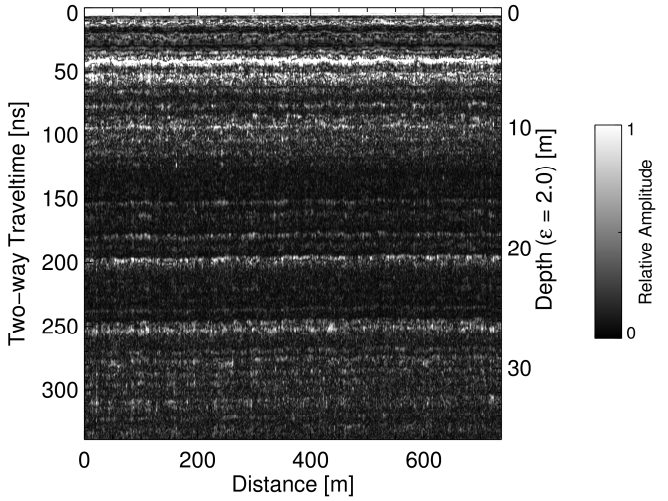

Fig. 1. Amplitude envelope of GPR profiles at South Dome, where several layers with varying backscattered power are visible.

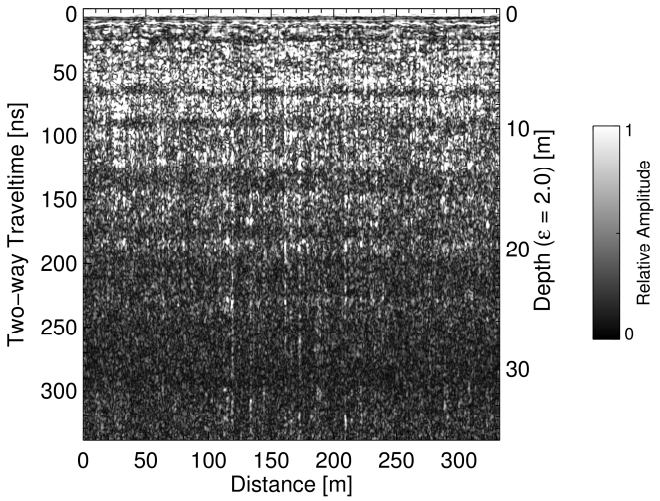

Fig. 2. Amplitude envelope of GPR profiles at EGIG T05, with a relatively homogeneous backscattering level that decreases with depth.

derived at different frequencies or polarizations. Fourth, the baseline dependence of the bias in order to account for DEMs acquired with different acquisition geometries.

The significant baseline dependence of the phase center depth was described under the assumption of a uniform volume (UV) model in [1]. Therefore, the penetration bias at the same time, space, frequency, and polarization is different at different baselines. The experimental validation of these findings is reported in Section III.

The relevant question is what model complexity is necessary to describe the baseline dependence and to compensate for the penetration bias. The modeling has to account for the vertical backscattering profile in the subsurface and should be applicable to different ice sheet conditions. The assumption of a uniform volume described by a constant scattering coefficient in the subsurface, the UV model, was first used by [10] to estimate penetration depths from the coherence magnitude, without the comparison to measured phase center depths. However, phase centers often appear deeper in experimental data than a UV model predicts [2], [11].

More recent studies have shown that a feasible approach for modeling the vertical backscattering profile in the subsurface of ice sheets is by combining a volume model with distinct subsurface layers represented by Dirac deltas [12]. A similar formulation with a UV model and boundaries above and below the volume, in the sense of air-snow and snow-firn interfaces, was used in [13] to describe Ka-band penetration into the snow cover at Greenland's summit. However, such approaches increase the parametric complexity of the vertical backscattering profile (i.e., the number of model parameters that need to be estimated) and make their inversion only possible in the context of fully polarimetric multi-baseline observation spaces. However, with respect to the estimation of the phase center depth, which requires only the estimation of the centroid of the vertical backscattering profile, the modeling can be simplified. Volume models, which are invertible also in lower dimensional observation spaces as single-baseline InSAR data, can approximate the phase center depth and its dependence on the baseline. This is supported by simulations of a combination of a volume model with distinct subsurface layers represented by Dirac deltas, which show a very similar phase center depth behavior as the pure volume models [2].

The goal of this paper is to quantify how accurately simple interferometric volume models can estimate and compensate the penetration bias in InSAR ice sheet surface elevations. The model complexity is purposely kept simple to enable model inversions by means of limited observation spaces (i.e. single-baseline (Pol-)InSAR acquisitions, typical for space borne SAR missions).

First, the phase center depth and its spatial baseline dependence is characterized at different frequencies and polarizations by using airborne InSAR data acquired at two different test sites on the Greenland ice sheet. The two test sites are characterized by different subsurface structures, which allow assessing the applicability of the investigated models to different scattering scenarios. Then the performance of UV model inversions to compensate the penetration bias is investigated. Approaches based on single channel as well as fully polarimetric InSAR data are discussed. An alternative, more flexible model, based on the Weibull function, is introduced and compared. The presented approaches address both random and oriented volume assumptions, since the vertical backscattering profiles in ice sheets were shown to be polarization dependent [14]. The accuracy of the penetration bias estimates is assessed against GNSS surface elevation measurements.

II. Data

Experimental airborne SAR data were acquired during the ARCTIC15 campaign in April and May 2015 on the Greenland ice sheet with DLR's F-SAR system. This study focusses on two test sites, both located in the percolation zone, but with different subsurface structures. The first test site, South Dome (63.52° N, 44.54° W, 2868 m a.s.l), experiences only limited melting during summer, which leads to refrozen

This article has been accepted for publication in a future issue of this journal, but has not been fully edited. Content may change prior to final publication. Citation information: DOI 10.1109/JSTARS.2020.2992530, IEEE Journal of Selected Topics in Applied Earth Observations and Remote Sensing

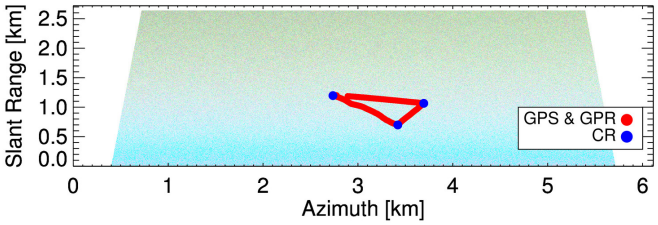

Fig. 3. Polarimetric image of the L-band data acquired at South Dome shown in the Pauli basis (HH+VV: blue, HH-VV: red, HV: green). The location of the ground measurements is indicated. Similar ground measurements are available at the EGIG T05 test site.

TABLE I
SOUTH DOME

Band	Freq. [GHz]	#Tracks	Nom. BL [m]	Res. Az. x Rg. [m]	k_{zVol}[rad/m]
X	9.6	9	2 – 35	0.5 x 0.5	0.11 – 4.8
C	5.3	7	5 – 35	0.5 x 0.5	0.15 – 2.6
L	1.3	6	5 – 30	0.6 x 1.3	0.04 – 0.58
P	0.44	8	10 – 270	1.0 x 3.8	0.05 – 2.1

EGIG T05

Band	Freq. [GHz]	#Tracks	Nom. BL [m]	Res. Az. x Rg. [m]	k_{zVol}[rad/m]
X	9.6	11	2 – 40	0.5 x 0.5	0.08 – 6.5
C	5.3	9	5 – 40	0.5 x 0.5	0.15 – 3.6
L	1.3	9	5 – 40	0.6 x 1.3	0.03 – 0.89
P	0.44	9	10 – 270	1.0 x 3.8	0.05 – 1.6

Summary of SAR acquisition parameters at both test sites. The nominal baselines are horizontal baselines flown at 3000 m above ground. At X-band, a second antenna provided an additional 1.7 m vertical baseline on two of the tracks. The azimuth and slant range resolution is single-look. The k_{zVol} range is indicated for the triangular track in Fig. 3.

ice inclusions within the firn that appear as layers at specific depths, which are visible in the ground penetrating radar (GPR) data in Fig. 1. The second test site, EGIG T05 (69.87° N, 47.13° W, 1938 m a.s.l), is characterized by an abundance of ice inclusions within the firn, due to more refrozen melt water because of its lower elevation. This leads to a more homogeneous vertical backscattering structure, clearly recognizable in the GPR data as shown in Fig. 2. The GPR data were acquired with a 500 MHz system along a triangular track in the scene center (see Fig. 3) with a maximum temporal separation of 14 days from the SAR acquisitions. They provide a qualitative characterization of the subsurface structure. Therefore, despite the nadir-looking acquisition geometry and the single frequency, they indicate the subsurface scattering properties for SAR acquisitions at larger incidence angles and higher frequencies. More information about the campaign can be found in [12] and [14].

In this study, fully polarimetric, multi-baseline SAR data at X-, C-, L-, and P-bands, acquired along six to nine parallel flight tracks are used. The acquisitions are summarized in Table I. The snow and firn conditions are considered stable during the acquisition period so that temporal decorrelation can be neglected [12]. The tomographic analysis of the data is discussed in [14]. The tomograms confirm the presence of dominant scattering layers at the South Dome test site, as also shown in the GPR data in Fig. 1. However, they also indicate a general volume backscattering distribution around the dominant layers. At the EGIG T05 test site, the tomograms in

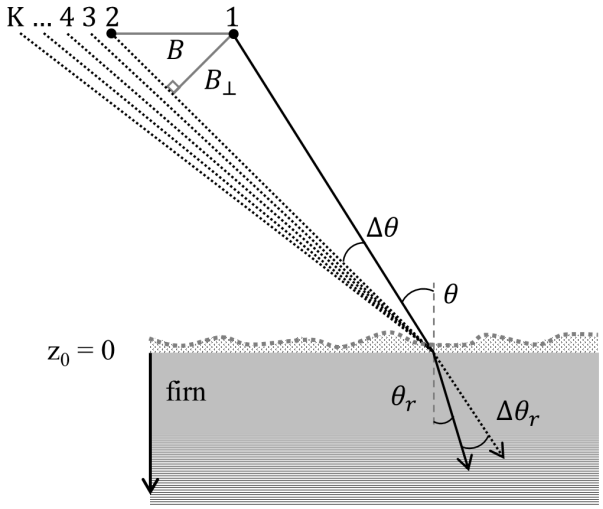

Fig. 4. Multi-baseline interferometric geometry with K acquisitions

[14] confirm the rather homogeneous subsurface scattering distribution, as also shown in the GPR data in Fig. 2.

GNSS measurements were performed on both test sites along a triangular path in the scene center, see Fig. 3, which provide the surface reference height. The interferometric phase centers are derived at the locations of the GNSS measurements covering incidence angles from 41° to 48° at South Dome and from 40° to 44° at EGIG T05. The corner reflectors were used to validate and refine the multi-baseline interferometric phase calibration [15].

III. BASELINE DEPENDENCE OF PHASE CENTERS

The interferometric phase $\angle\gamma$ is derived from the complex interferometric coherence γ

$$\gamma(\vec{w}) = \frac{\langle s_1(\vec{w}) s_2^*(\vec{w})\rangle}{\sqrt{\langle s_1(\vec{w}) s_1^*(\vec{w})\rangle \langle s_2(\vec{w}) s_2^*(\vec{w})\rangle}} \quad (1)$$

obtained from the interferometric image pair s_1 and s_2 at polarization $\vec{w}$ [16]. The phase center location is given by $\angle\gamma / k_{zVol}$, where the vertical wavenumber k_{zVol} is [17]

$$k_{zVol} = \frac{4\pi\sqrt{\epsilon_r}}{\lambda} \frac{\Delta\theta_r}{sin\theta_r}, \quad (2)$$

which describes the variation of the interferometric phase $\angle\gamma$ as a function of depth z. The permittivity of the volume ϵ_r is set to 2.0 for this analysis based on its relationship to density [18] measured in firn cores [19]. λ is the wavelength in free space. θ_r is the refracted incidence angle within the firn volume. $\Delta\theta_r$ is the difference in θ_r introduced by the spatial baseline between the acquisitions, as depicted in Fig. 4.

After conventional InSAR processing and without temporal decorrelation, the coherence γ depends on the vertical backscattering profile $\sigma_v(z)$

$$\gamma(\vec{w}) = e^{ik_z z_0} \frac{\int_{-\infty}^{0} \sigma_v(z,\vec{w}) e^{ik_{zVol} z} dz}{\int_{-\infty}^{0} \sigma_v(z,\vec{w}) dz}. \quad (3)$$

This article has been accepted for publication in a future issue of this journal, but has not been fully edited. Content may change prior to final publication. Citation information: DOI 10.1109/JSTARS.2020.2992530, IEEE Journal of Selected Topics in Applied Earth Observations and Remote Sensing

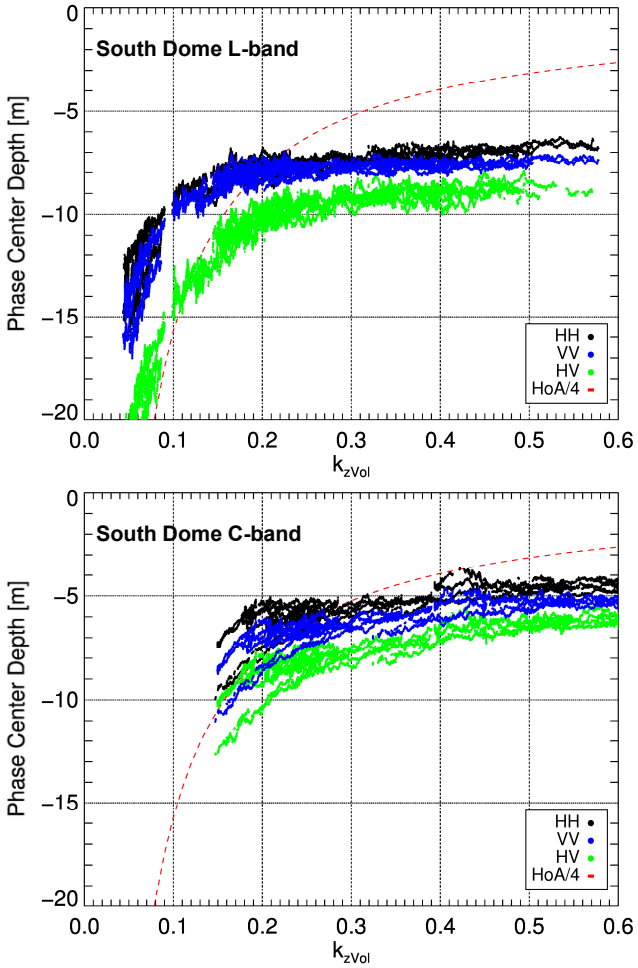

Fig. 5. Phase center depths referenced to GNSS measurements from several baselines of the South Dome data at L-band (top) and C-band (bottom) in three polarizations. The lower theoretical limit, $HoA/4$, of a UV model is also shown.

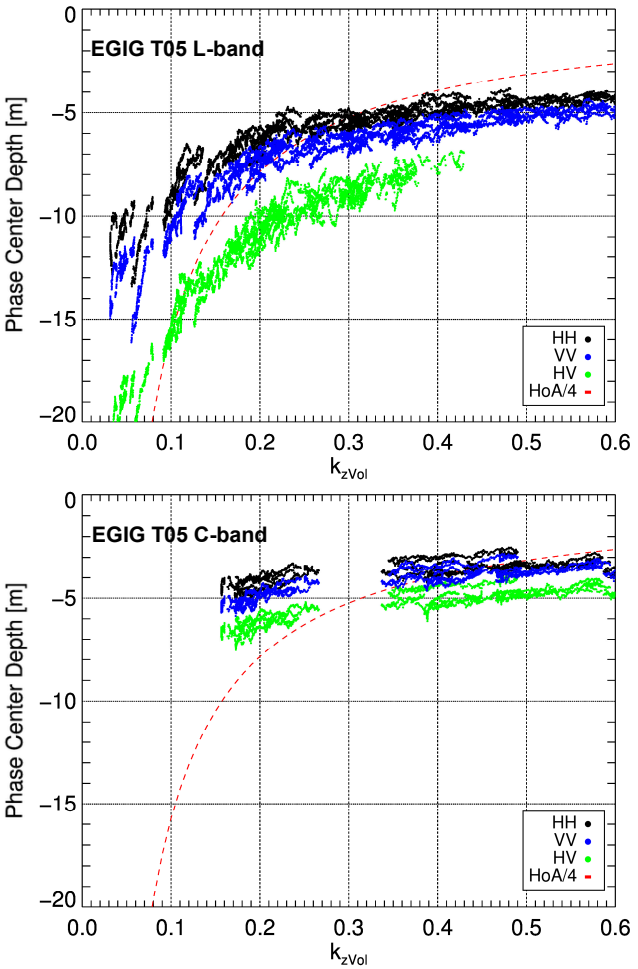

Fig. 6. Phase center depths referenced to GNSS measurements from several baselines of the EGIG T05 data at L-band (top) and C-band (bottom) in three polarizations. The lower theoretical limit, $HoA/4$, of a UV model is also shown.

The depth of the phase center is related to the effective centroid of the vertical backscattering profile $\sigma_v(z)$ in the subsurface, while the magnitude of the interferometric coherence is related to the vertical spread of $\sigma_v(z)$. In an oriented volume scenario, $\sigma_v(z)$ depends on polarization $\vec{w}$, while $\sigma_v(z)$ is independent of $\vec{w}$ for a random volume.

The interferometric phase is referenced to corner reflectors and GNSS measurements at the surface. The surface is defined at $z_0 = 0\,m$ so that the phase center location $\angle\gamma/k_{zVol}$ is directly given by the phase center depth, which is equal to the penetration bias of an InSAR DEM. The phase centers are measured at the locations of the GNSS measurements (see Fig. 3) at a wide range of k_{zVol}. Small k_{zVol} variations arise from the incidence angle variation across the GNSS locations within a single interferogram. In addition, larger k_{zVol} variations are achieved by using interferograms at different baselines. The analysis is restricted to samples with $k_{zVol} < 0.6$ and $|\gamma| > 0.1$.

The phase center depths shown in Fig. 5 for South Dome L- and C-band data at HH, VV, and HV polarizations are derived from multiple baselines which overlap in their k_{zVol}-range. The L-band phase centers at small k_{zVol} are up to a factor of 2 deeper than at larger k_{zVol}, even though they are from the same GNSS locations. In this case, the variation in interferometric baseline changes the penetration bias by up to 10 m. The baseline dependence leads to a strong phase center depth variation mainly for $k_{zVol} < 0.2$, with a more stable behavior at higher k_{zVol}. The co-polarized channels are very similar and the VV phase centers are about 1 m deeper than at HH. In contrast, the HV phase centers are 3-7 m deeper.

At South Dome, phase centers at C-band can be derived only for $k_{zVol} > 0.15$ with the available baselines. They are about 2-3 m closer to the surface than at L-band, but the difference is expected to be larger for smaller k_{zVol}.

Phase center depths at the EGIG T05 test site in L- and C-band are shown in Fig. 6. They appear less densely sampled than at South Dome because a smaller amount of GNSS measurements was acquired at EGIG T05. This is related to a shorter GNSS track, which leads also to a smaller k_{zVol} variation for each baseline, causing gaps in k_{zVol}. The EGIG T05 phase center depths are on average 1-2 m closer to the surface than their South Dome counterparts. This comes from

This article has been accepted for publication in a future issue of this journal, but has not been fully edited. Content may change prior to final publication. Citation information: DOI 10.1109/JSTARS.2020.2992530, IEEE Journal of Selected Topics in Applied Earth Observations and Remote Sensing

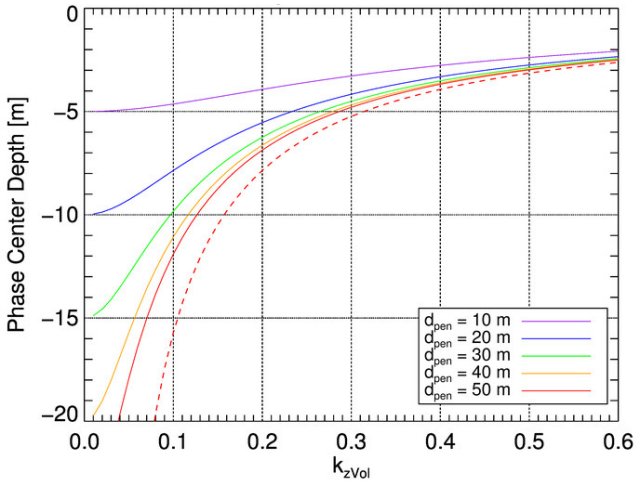

Fig. 7. Simulated phase center depths for the UV model with different d_{pen}.

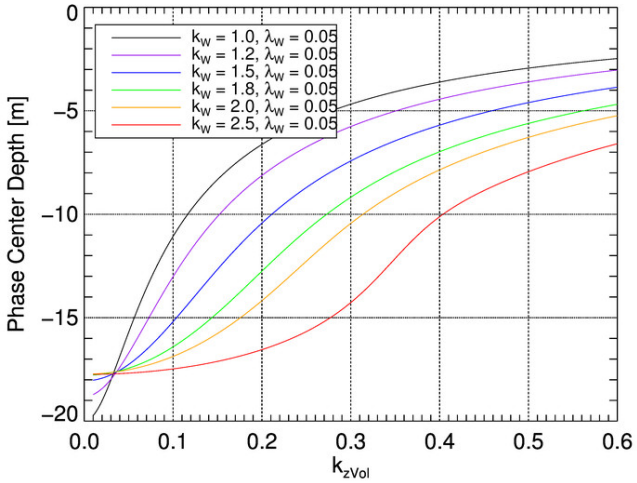

Fig. 8. Simulated phase center depths for a Weibull model with $\lambda_w = 0.05$ and varying k_w.

the larger amount of refrozen ice inclusions in the subsurface, which leads to a more homogeneous scattering closer to the surface than at South Dome [14]. This homogeneous subsurface scattering behavior fits better to the assumptions of the UV model, therefore the EGIG T05 L-band phase centers follow closer the UV model indicated by the red dashed line. The EGIG T05 L-band phase center depths at HV at higher k_{zVol} values are not shown as their coherence magnitudes are below 0.1.

The baseline dependence is the result of the Fourier transform of a non-symmetric $\sigma_v(z)$ in (3), which is complex valued and has a phase that changes with sampling frequency k_{zVol} [20]. A more descriptive interpretation is in terms of the phase wrapping of deeper scattering contributions with increasing k_{zVol}. Accordingly, deeper scatterers contribute with the same phase as scatterers just below the surface. This moves the phase center depth upwards with increasing k_{zVol}. Phase centers of a UV model cannot be deeper than a quarter of the height of ambiguity, due to this effect [1]. This limit is also shown by the red dashed line in Fig. 5 and Fig. 6. The phase centers roughly follow the theoretical limit, but are often deeper than the UV model predicts.

Note that there are small, but visible, residual phase offsets in the data. For instance, the two "lines" at each polarization in the South Dome C-band phase center depths in Fig. 5 at $k_{zVol} = 0.15$ come from two different baselines, which cover the same k_{zVol} range. The difference of about 2 m between the phase center depths derived from these two baselines is due to a residual phase offset. Similar, but smaller effects are also visible in the other data sets, for instance the small deviations of less than 1 m at $k_{zVol} = 0.13$ visible in the South Dome L-band data. All coherences were estimated using at least 2298 looks to ensure accurate phase estimates. The resulting standard deviation of the phase center depth estimates is on average 0.14 m with a worst case of 0.70 m at P-band. The estimation window size is maximum 111 m x 82 m (slant range x azimuth), which is feasible due to the spatial homogeneity of the test sites.

IV. Modeling and Inversion

Simulations of the vertical backscattering profile with the UV model [10] and the Weibull [14] model are used to investigate the modeling and compensation of the penetration bias. For the UV model, a single-polarization and full-polarization inversion are tested. For the Weibull model, a full-polarization inversion is analyzed, as its complexity does not allow a single-polarization inversion.

A. Uniform Volume Model

Assuming a uniform volume of scatterers with a constant extinction coefficient $\kappa_e(\vec{w})$ [10], the vertical backscattering function $\sigma_v(z)$ in (3) becomes exponential

$$\sigma_{uv}(z,\vec{w}) = \sigma_v^0(\vec{w})\mathrm{e}^{\frac{2z\kappa_e(\vec{w})}{cos\theta_r}} = \sigma_v^0(\vec{w})\mathrm{e}^{\frac{2z}{d_{pen}(\vec{w})}}, \quad (4)$$

where $\sigma_v^0(\vec{w})$ is the nominal backscatter power per unit volume at a given polarization $\vec{w}$ and the extinction coefficient $\kappa_e(\vec{w})$ accounts for both scattering and absorption losses. Parameterizing with the one-way penetration depth d_{pen}, which is inversely related to κ_e through $\kappa_e = cos(\theta_r)/d_{pen}$ and inserting (4) into (3) leads to γ_{uv} for a UV model [10]

$$\gamma_{uv}(\vec{w}) = e^{ik_z z_0}\frac{1}{1+\frac{id_{pen}(\vec{w})k_{zVol}}{2}}. \quad (5)$$

The phase center depths for a UV model are shown in Fig. 7, simulated for different d_{pen} and $z_0 = 0\,m$. A stronger baseline dependence for deeper penetration is indicated, which agrees with the stronger baseline dependence of the deeper HV phase centers in Fig. 5 and Fig. 6.

B. Weibull Volume Model

The Weibull function allows more flexible shapes for the vertical profile with

$$\sigma_w(z) = \lambda_w k_w(\lambda_w z)^{k_w-1}e^{-(\lambda_w z)^{k_w}}. \quad (6)$$

This article has been accepted for publication in a future issue of this journal, but has not been fully edited. Content may change prior to final publication. Citation information: DOI 10.1109/JSTARS.2020.2992530, IEEE Journal of Selected Topics in Applied Earth Observations and Remote Sensing

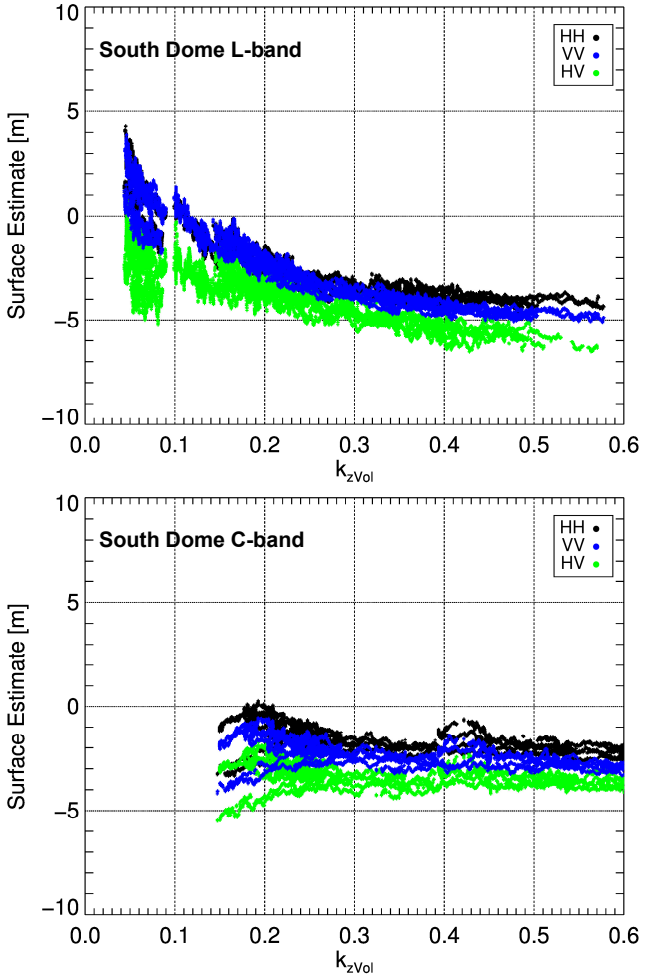

Fig. 9. UV surface estimates from South Dome L-band (top) and C-band (bottom) coherences from single channel UV inversions limited to $|\gamma| > 0.1$.

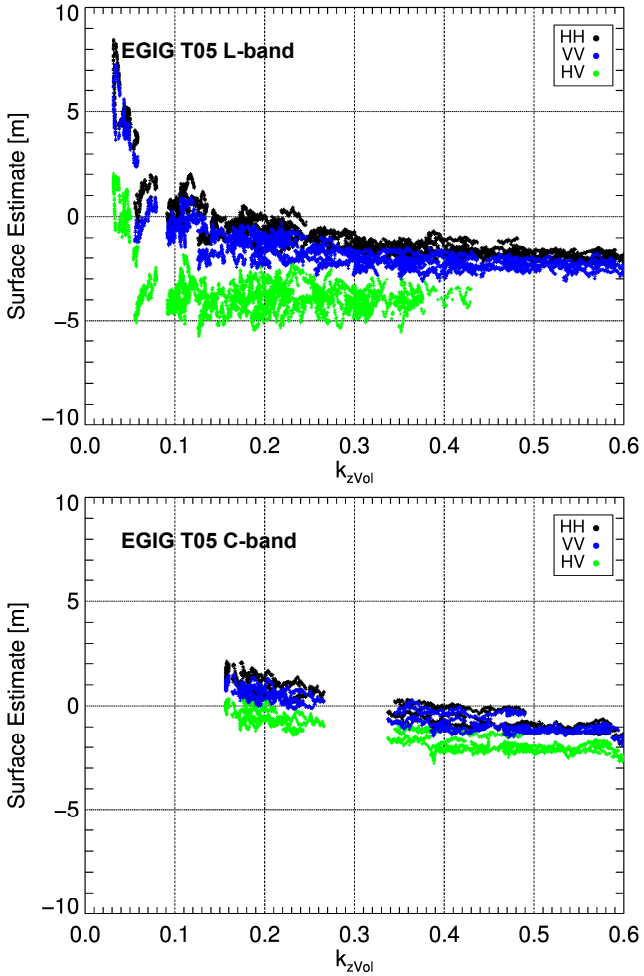

Fig. 10. UV surface estimates from EGIG T05 L-band (top) and C-band (bottom) coherences from single channel UV inversions limited to $|\gamma| > 0.1$.

The scale parameter λ_w is similar, but not identical, to the extinction coefficient $\kappa_e(\vec{w})$ in (4). k_w is the shape parameter and $k_w = 1$ leads to an exponential, $k_w = 2$ to a Rayleigh distribution and $k_w \approx 3.6$ approximates a Gaussian. The integrals in (3) are numerically solved in the interval $[0, \infty]$ using (6), as closed form solutions are only available for particular k_w values.

Simulated phase center depths for varying k_w of the Weibull model are shown in Fig. 8. It is evident that the two model parameters of the Weibull function, compared to one parameter in the UV model, increase the flexibility in describing the baseline dependence of phase center depths.

C. Uniform Volume Inversion

The inversion of the penetration bias using the UV model is straight forward. While the phase center depth obviously depends on the penetration depth d_{pen}, see Fig. 7, the relationship between the phase $\angle\gamma_{uv}$ and the magnitude $|\gamma_{uv}|$ of the complex coherence is always the same and describes a semi-circle in the unit circle, given by the black line in Fig. 12. As a result, $\angle\gamma_{uv}$ can be derived from $|\gamma_{uv}|$ independently of d_{pen} [1]

$$\angle\gamma_{uv} = tan^{-1}\left(\sqrt{\frac{1}{|\gamma_{uv}|^2} - 1}\right). \quad (7)$$

This allows the estimation of the phase from only a single coherence magnitude. The compensation of the penetration bias is then performed by subtracting this phase term from the measured phase.

Results from single channel UV inversions are shown for the South Dome data in Fig. 9. The surface estimates, despite being not exactly at $z = 0\,m$, still provide more accurate topographic information than the corresponding phase centers in Fig. 5. The baseline dependence is partially compensated. At L-band, the UV model predicts a stronger baseline dependence than what is found in the data, which can be seen by comparing the simulations in Fig. 7 with Fig. 5. Therefore, while the phase center depths around $k_{zVol} = 0.1$ in Fig. 5 are accurately compensated with surface estimates around 0 m in Fig. 9, the surface estimates at higher k_{zVol} values are still a few meters below the surface. For instance, the UV model predicts only 2.5 m at $k_{zVol} = 0.6$, so that the HH phase center depths of -6.5 m in Fig. 5 can only be compensated to a surface estimate at -4 m in Fig. 9. The surface estimates based on the single channel UV inversion are even overestimated at the smaller k_{zVol} values. In contrast, the baseline dependence

This article has been accepted for publication in a future issue of this journal, but has not been fully edited. Content may change prior to final publication. Citation information: DOI 10.1109/JSTARS.2020.2992530, IEEE Journal of Selected Topics in Applied Earth Observations and Remote Sensing

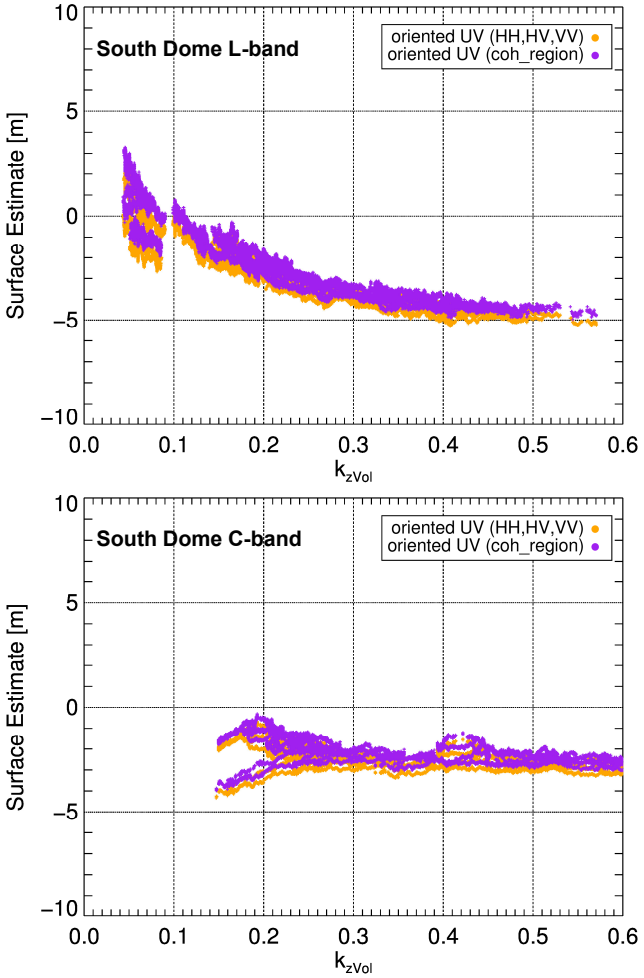

Fig. 11. Surface estimates from South Dome L-band (top) and C-band (bottom) coherences with the oriented volume UV inversion limited to $|\gamma| > 0.1$, based on fully polarimetric InSAR data.

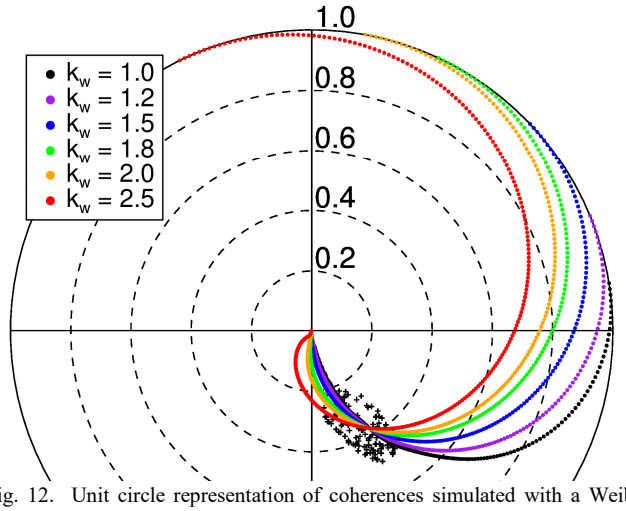

Fig. 12. Unit circle representation of coherences simulated with a Weibull model and fitted to an example coherence region from the South Dome L-band data (black crosses). $k_w = 1.0$ (black line), corresponds to a UV model.

of the South Dome C-band phase center depths (Fig. 5) is accurately compensated by the UV surface estimates in Fig. 9 and the UV surface estimates are clearly closer to the surface. Residual differences between polarizations remain.

The results from the UV model inversions for the EGIG T05 data are shown in Fig. 10. The EGIG T05 UV surface estimates at L-band show a better removal of the baseline dependence for $k_{zVol} > 0.1$ than at South Dome, which was expected, because the phase center depths agree better with the behavior of the UV model. In contrast, the overestimation of the surface location at smaller k_{zVol} values is even stronger. At C-band, the penetration bias and its baseline dependence is compensated to a large extent and some of the co-polarized estimates are at the surface at $z = 0\,m$. The set of surface estimates based on the baseline that provides the samples around $k_{zVol} = 0.2$ is slightly overestimated.

The surface location is, for small k_{zVol} values, overestimated in the L-band data at both test sites and a residual baseline dependence remains visible. In a general sense, it appears that there are scattering components that the modeled vertical backscattering profile $\sigma_v(z)$ does not account for. The fact that the residual trend is similar in the data from both test sites contradicts an explanation based on the distinct subsurface layers at the South Dome test site. Additionally, simulations with Dirac deltas for the subsurface layers do not show the observed behavior. The origin appears to be the dominant role of the coherence magnitude $|\gamma|$ in the model inversion: any deviation from the assumed exponential profile is fitted in terms of $|\gamma|$ at the cost of a larger deviation in the phase $\angle\gamma$. Due to this, at small k_{zVol} values in the L-band data, the UV inversion predicts a too large phase term in (7) based on $|\gamma|$, leading to overestimated surface locations (Fig. 9 and Fig. 10).

The effect of the residual phase offsets, mentioned in Section III, are again visible in Fig. 9 as differences of 1-2 m between the sets of surface estimates derived from different baselines. A slightly different residual phase calibration effect is visible in the surface estimates with the UV model for the EGIG T05 L-band data in Fig. 10. The set of samples from one baseline that is around $k_{zVol} = 0.08$ is on average consistent with the results from other baselines, but shows an opposing trend within the set of samples.

Note that the use of a permittivity value of $\epsilon_r = 2.0$, based on density information, for the calculation of k_{zVol} in (2) is not critical for the trends in the surface estimations. The effect of ϵ_r is largely compensated by the respective change in refracted incidence angle in (2). Even the use of extreme values of 1 (permittivity of air) and 3.15 (permittivity of solid glacier ice) shift the phase center depths and the surface estimations only by about 1 m with only a marginal effect on the trend.

The UV model inversion can be straight forwardly applied to a fully polarimetric observation space. Averaging the surface estimates from the UV inversion across different polarizations gives essentially the surface estimate of an oriented uniform volume with polarization dependent $d_{pen}(w)$. In the following we use the term "oriented" to characterize polarization dependent vertical backscattering profiles. The surface estimation with an oriented UV model is shown in Fig. 11 and was applied first only on HH, VV, and HV polarizations, and second, by exploiting the full

This article has been accepted for publication in a future issue of this journal, but has not been fully edited. Content may change prior to final publication. Citation information: DOI 10.1109/JSTARS.2020.2992530, IEEE Journal of Selected Topics in Applied Earth Observations and Remote Sensing

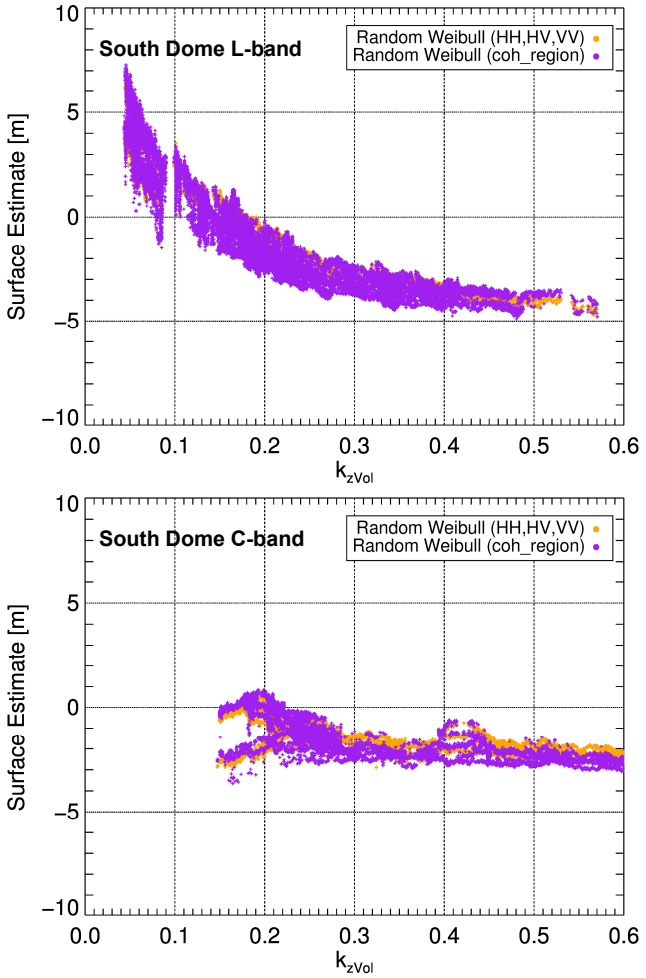

Fig. 13. Surface estimates from South Dome L-band (top) and C-band (bottom) coherences with the Weibull inversion constrained to $k_w < 1.2$, based on fully polarimetric InSAR data.

polarimetric space of the coherence region, by randomly sampling $\vec{w}$ in (1) [16]. The oriented UV inversion is similar to the single-polarization result in Fig. 9, but clearly reduces the variability due to polarizations. Interestingly, the results barely differ between the inversion based on only HH, VV, and HV or the coherence region. The results based on the coherence region are only slightly higher, because the coherence regions are more densely populated around the HH and VV coherence loci, which leads to a stronger weighting of these polarization states.

A. Weibull model inversion

The Weibull model leads to a more challenging inversion problem. An oriented Weibull model, where both k_w and λ_w can vary with polarization, is not invertible with full polarimetric single-baseline InSAR data.

The tomographic analysis in [14] motivates the idea that the shape k_w is identical across polarizations and only λ_w varies. This can be exploited because numerical results show that the shape of the line of Weibull coherences in the unit circle depends only on k_w, while λ_w and k_{zVol} move the coherences along the line defined by k_w, as shown in Fig. 12.

Therefore, while the phase $\angle\gamma_w$ depends on the Weibull model, cf. Eq. (6),

$$\angle\gamma_w = f(k_w, \lambda_w, k_{zVol}, z_0), \tag{8}$$

when considering coherence magnitudes $|\gamma_w|$, it can be reduced to

$$\angle\gamma = f(k_w, |\gamma_w|, z_0). \tag{9}$$

Unfortunately, no analytic solution could be established for (9). However, the slope between $\angle\gamma$ and $|\gamma|$ for coherences measured at different polarizations can be compared to the same slope of simulated coherences in the respective $|\gamma|$ range. In this way, an estimate of the k_w parameter can be obtained by minimizing the difference in this slope between the data and simulations. The difference in phase between the complex mean of the measured and the simulated coherences in the $|\gamma|$-range of interest provides then the surface estimate $\hat{z}_0$.

Higher k_w parameters produce shapes of the Weibull coherences in the unit circle that overestimate the surface phase. This effect is visible in Fig. 12, when comparing the distance between the coherence region (black crosses) and the surface phase (intersection with the unit circle) of e.g. the red line. Constraining $k_w < 1.2$ is required for achieving reasonable results. Fig. 13 shows surface estimates with the Weibull inversion for the South Dome L- and C-band data based on HH, HV, and VV coherences as well as on full coherence regions, which largely overlap. The general behavior is similar to the oriented volume UV inversion in Fig. 11. At C-band, the Weibull results are slightly closer to the surface and the baseline dependence is equally good removed. However, at L-band, the surface is overestimated for small k_{zVol}, while for larger k_{zVol} the estimates are slightly closer to the surface than the UV estimates in Fig. 11. Similar observations can be made for the Weibull inversion of the EGIG T05 phase centers, which are not shown here.

V. Results

The phase center depths are compared to the surface estimates of the three investigated inversions in Fig. 14. The statistics are derived for all results with $k_{zVol} < 0.6$, which is the expected k_{zVol} range for the mission concept Tandem-L [21], and $|\gamma| > 0.1$. For instance, the boxplots of the phase center depths at South Dome in L-band in Fig. 14 are derived from the measurements shown in Fig. 5 (top). The upper and lower quartiles as well as the maximum and minimum values indicate the variability in the results including the baseline dependence.

The phase center depths show the expected behavior with deeper phase centers at longer wavelengths and in the HV channel compared to shorter wavelengths and the co-polarized channels, respectively. At X- and C-band, as expected, the phase centers at EGIG T05 are closer to the surface than at South Dome, because of the more homogeneous scattering

This article has been accepted for publication in a future issue of this journal, but has not been fully edited. Content may change prior to final publication. Citation information: DOI 10.1109/JSTARS.2020.2992530, IEEE Journal of Selected Topics in Applied Earth Observations and Remote Sensing

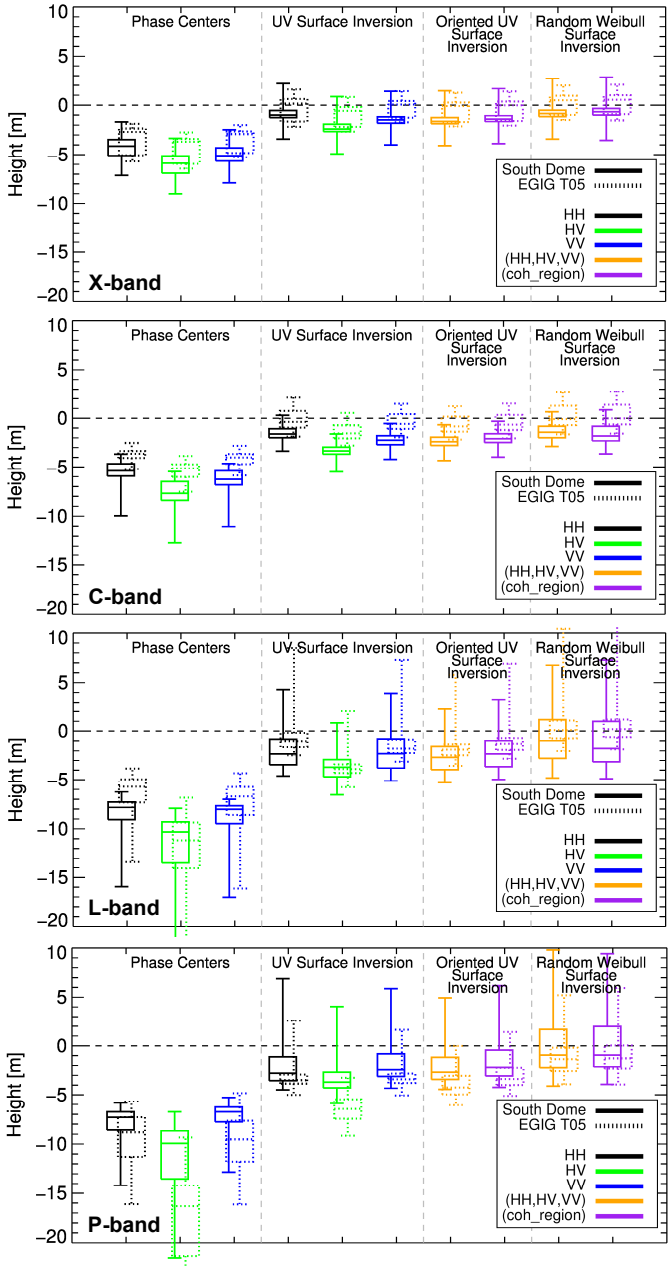

Fig. 14. Boxplots (Max, upper quartile, median, lower quartile, min) of the phase centers and different surface estimates at the South Dome and EGIG T05 test sites. From top to bottom: X-, C-, L-, and P-band. The Weibull inversion was constrained to $k_w < 1.2$.

behavior closer to the surface at EGIG T05, which is indicated by the GPR data (Fig. 2) and tomograms [14]. This applies also to the co-polarized channels at L-band, but is the opposite for P-band. The subsurface at South Dome is characterized by dominant scattering layers, with very similar vertical backscattering profiles in L- and P-band [14]. This leads to very similar L- and P-band phase center depths, while the more homogeneous subsurface at EGIG T05 leads to P-band penetrating deeper than L-band.

The single-polarization inversion of the UV model provides already a good compensation of the median phase center depth and gives surface estimates which are only few meters below the real surface. Also the baseline dependence is reduced and the inversion results show a smaller variability than the phase center depths. The variability is further reduced by applying the oriented volume UV inversion to the interferometric coherences of all polarization channels.

The Weibull inversion needs to be constrained to $k_w < 1.2$ in order to limit overestimation. The Weibull inversions have a slightly larger variation in the surface estimates because of its tendency to overestimate the distance between the phase center and the surface, while the median values are closer to the real surface than for the UV inversions. The Weibull model therefore presents a way to account for the slight underestimation of the UV model, but is also prone to overestimation.

VI. Discussion and Conclusion

The single-polarization UV inversion, which can be applied to any InSAR coherence, provides more accurate surface elevation than obtained from the measured interferometric phase center. For instance, the median value of the phase center depth of the South Dome L-band HH data in Fig. 14 is -7.8 m, while the median of the UV surface estimates is -2.3 m. This corresponds to a significant reduction in the penetration bias of an InSAR DEM. On average, the penetration bias is reduced by a factor of 2.5 to 6.5 in the investigated data. The variability of the UV surface estimates is reduced compared to the variability of the measured phase center depths. The compensation of the baseline dependence with a UV model is demonstrated. The remaining uncertainties come from a residual baseline dependence but also from the variance in the experimental data. A further reduction of the variability can be achieved by applying an oriented volume UV inversion to polarimetric InSAR data. This combines the information from different polarizations and improves the result.

The Weibull inversion is introduced for a more flexible representation of the shape of the vertical backscattering profile. This is helpful in cases where the UV model underestimates the surface location, because the Weibull model allows larger distances between the surface and the phase center. However, the Weibull inversion can overestimate the surface, making a constraint on the Weibull shape parameter k_w necessary. The Weibull model shows potential for better surface estimation than the UV model, but its inversion still needs to be improved.

Interestingly, the oriented volume UV and Weibull inversions perform very similarly based on the HH, HV, and VV coherences and based on a densely sampled coherence region even though the latter theoretically has a larger information content.

The baseline dependence of the phase center depths can be approximated with pure volume models even in the presence of distinct subsurface scattering layers. This was already indicated by simulations [2] and can be recognized when comparing the phase center depths of the South Dome data (see Fig. 5) with the volume model simulations (see Fig. 7 and Fig. 8).

Given the performance of the UV inversion and because it can be applied to any single-polarization interferometric coherence, the main conclusion is that UV surface estimations should be preferred over the sole phase center information, as long as other decorrelation sources, e.g. temporal decorrelation, can be neglected or accounted for.

This is particularly true for the compensation of the absolute value of the penetration bias, in case InSAR DEMs are compared to other sources of surface elevation. If two InSAR DEMs acquired at different dates are compared, only the temporal difference of the penetration bias is relevant. For instance, if the subsurface structure would change from the scenario at South Dome, due to increased melting, to a subsurface structure similar to the EGIG T05 test site, the difference in the average penetration bias in L-band in HH would be 2.1 m, which would propagate directly as an error in the elevation change estimation. This error can be reduced by 40% with the single polarization UV model inversion and by over 50% with the fully polarimetric UV inversion. In general, the differences in the phase center depths of the two test sites are always larger than the differences in the model-based surface estimates at all frequencies and polarizations. Therefore, the model-based compensation of the penetration bias also improves the accuracy of surface elevation changes estimated from InSAR DEM differencing. The same applies even more to InSAR DEMs acquired at different frequencies or polarizations. If InSAR DEMs are generated at the same snow and ice conditions and with the same acquisitions parameters, except for a difference in baseline, which is a likely scenario for space borne SAR, only the baseline dependence of the penetration bias is relevant. The presented model inversions are able to compensate this effect to a varying extent depending on the frequency.

One has to accept that, depending on the frequency, in dry and frozen conditions, the first few meters of snow and firn can be transparent. Tomographic analyzes indicated that the thickness of this transparent part is between 1 m at X-band and 5 m at L- and P-bands in the investigated data [14]. Nevertheless, the inversion of a "radar surface", which ignores this transparent part, provides more reliable topographic information over ice sheets than using the pure interferometric phase center information. The simple volume models investigated in this paper demonstrate the compensation of the penetration bias in InSAR DEMs. However, models of higher complexity could account for more aspects of subsurface scattering and improve the estimation performance, but their inversion requires also higher dimensional observation spaces. This could be addressed in the context of future SAR missions [21] that are able to provide polarimetric InSAR measurements of the same area at multiple baselines within few weeks.

ACKNOWLEDGMENT

The authors would like to thank everyone involved in the ARCTIC15 campaign, which was conducted by DLR and ETH Zurich in cooperation with the Danish Defence Acquisition and Logistics Organization (DALO). They would also like to thank the anonymous reviewers for the valuable and constructive comments, which improved the clarity of this paper.

REFERENCES

[1] J. Dall, "InSAR Elevation Bias Caused by Penetration Into Uniform Volumes," IEEE Transactions on Geoscience and Remote Sensing, vol. 45, no. 7, pp. 2319–2324, Jul. 2007.

[2] G. Fischer, G. Parrella, K. P. Papathanassiou, and I. Hajnsek, "Sensitivity of polarimetric SAR interferometry data to different vertical subsurface structures of the Greenland ice sheet," in Proc. of IGARSS, Forth Worth, USA, 2017, pp. 3581–3584.

[3] B. Wessel, A. Bertram, A. Gruber, S. Bemm, and S. Dech, "A New High-Resolution Elevation Model of Greenland Derived from Tandem-X," ISPRS Annals of Photogrammetry, Remote Sensing and Spatial Information Sciences, vol. III–7, pp. 9–16, Jun. 2016.

[4] J. Dall, S. N. Madsen, K. Keller, and R. Forsberg, "Topography and penetration of the Greenland Ice Sheet measured with Airborne SAR Interferometry," Geophysical Research Letters, vol. 28, no. 9, pp. 1703–1706, May 2001.

[5] E. Rignot, K. Echelmeyer, and W. Krabill, "Penetration depth of interferometric synthetic aperture radar signals in snow and ice," *Geophys. Res. Lett*., vol. 28, no. 18, pp. 3501–3504, Sep. 2001.

[6] J. Gardelle, E. Berthier, Y. Arnaud, and A. Kääb, "Region-wide glacier mass balances over the Pamir-Karakoram-Himalaya during 1999-2011," *The Cryosphere*, vol. 7, no. 4, pp. 1263–1286, Aug. 2013.

[7] H. Rott, W. A. Jaber, J. Wuite, S. Scheiblauer, D. Floricioiu, J. M. van Wessem, T. Nagler, N. Miranda, and M. R. van den Broeke, "Changing pattern of ice flow and mass balance for glaciers discharging into the Larsen A and B embayments, Antarctic Peninsula, 2011 to 2016," *The Cryosphere*, vol. 12, no. 4, pp. 1273–1291, Apr. 2018.

[8] W. Abdel Jaber, H. Rott, D. Floricioiu, J. Wuite, and N. Miranda, "Heterogeneous spatial and temporal pattern of surface elevation change and mass balance of the Patagonian icefields between 2000 and 2016," *The Cryosphere Discussions*, pp. 1–39, Dec. 2018.

[9] S. Abdullahi, B. Wessel, M. Huber, A. Wendleder, A. Roth, and C. Kuenzer, "Estimating Penetration-Related X-Band InSAR Elevation Bias: A Study over the Greenland Ice Sheet," in *Remote Sens*., vol. 11, no. 24, pp. 1-19, Dec. 2019.

[10] E. W. Hoen and H. Zebker, "Penetration depths inferred from interferometric volume decorrelation observed over the Greenland ice sheet," *IEEE Trans. Geosci. Remote Sens*., vol. 38, no. 6, pp. 2572–2583, Nov. 2000.

[11] J. Dall, K.P. Papathanassiou, and H. Skriver, "Polarimetric SAR interferometry applied to land ice: Modeling," in *Proc. EUSAR*, Ulm, Germany, 2004, pp. 247-250.

[12] G. Fischer, K. P. Papathanassiou and I. Hajnsek, "Modeling Multifrequency Pol-InSAR Data From the Percolation Zone of the Greenland Ice Sheet," in *IEEE Trans. Geosci. Remote Sens*., vol. 57, no. 4, pp. 1963-1976, April 2019.

[13] S. Hensley, D. Moller, S. Oveisgharan, T. Michel, and X. Wu, "Ka-Band Mapping and Measurements of Interferometric Penetration of the Greenland Ice Sheets by the GLISTIN Radar," in *IEEE J. Sel. Topics Appl. Earth Observ. Remote Sens.*, vol. 9, no. 6, pp. 2436–2450, Jun. 2016.

[14] G. Fischer, M. Jäger, K. P. Papathanassiou, and I. Hajnsek, "Modeling the Vertical Backscattering Distribution in the Percolation Zone of the Greenland Ice Sheet with SAR Tomography" in *IEEE J. Sel. Topics Appl. Earth Observ. Remote Sens.,* vol. 12, no. 11, pp. 4389–4405, Nov. 2019.

[15] M. Jäger, R. Scheiber, and A. Reigber, "External Calibration of Multi-Channel SAR Sensors Based on the Pulse-by-Pulse Analysis of Range Compressed Data," in *Proc. EUSAR*, Aachen, Germany, Jun. 2018, pp. 75–78.

[16] S.R. Cloude and K.P. Papathanassiou, "Polarimetric SAR interferometry," *IEEE Trans. Geosci. Remote Sens.*, vol. 36, no. 5, pp. 1551-1565, Sept. 1998.

[17] J.J. Sharma, I. Hajnsek, and K.P. Papathanassiou, "Estimation of glacier ice extinction using long-wavelength airborne Pol-InSAR," *IEEE Trans. Geosci. Remote Sens.*, vol. 51, no. 6, pp. 3715-3732, Jun. 2013.

[18] C. Mätzler, "Applications of the interaction of microwaves with the natural snow cover," *Remote Sensing Rev.*, vol. 2, pp. 259-387, 1987.

[19] J. Freitag, S. Kipfstuhl, S. Hoerz, L. Eling, B. Vinther, and T. Popp, "Melt layer statistic of two firn cores recently drilled at Dye3 and South Dome in the dry snow zone of southern Greenland", presented at EGU General Assembly, Vienna, Austria, Apr. 27–May 2, 2014.

[20] R. N. Bracewell, The Fourier transform and its applications, 3rd ed. Boston: McGraw Hill, 2000.

[21] A. Moreira, G. Krieger, I. Hajnsek, K. Papathanassiou, M. Younis, P. Lopez-Dekker, S. Huber, M. Villano, M. Pardini, M. Eineder, F. De Zan, and A. Parizzi, "Tandem-L: A Highly Innovative Bistatic SAR Mission for Global Observation of Dynamic Processes on the Earth's Surface," IEEE Geoscience and Remote Sensing Magazine, vol. 3, no. 2, pp. 8–23, Jun. 2015.